Vibration Frequencies of $Mg_3Al_2Si_3O_{12}$ Pyrope. An ab Initio Study with the CRYSTAL Code

Fabien Pascale,[†] Claudio M. Zicovich-Wilson,[‡] Roberto Orlando,*[,§] Carla Roetti,[||] Piero Ugliengo,[||] and Roberto Dovesi[||]

Laboratoire de Cristallographie et Modélisation des Matériaux Minéraux et Biologiques, Université Henri Poincaré, BP 239, 54506 Vandoeuvre les Nancy Cedex, France, Universidad Autónoma del Estado de Morelos, Av. Universidad 1001, Col. Chamilpa, 62210 Cuernavaca (Morelos), Mexico, Dipartimento di Scienze e Tecnologie Avanzate, Università del Piemonte Orientale, Via Bellini 25/G, 15100 Alessandria, Italy, and Dipartimento di Chimica IFM, Università di Torino, Via P. Giuria 5, 10125 Torino, Italy

Received: January 18, 2005

The vibrational spectrum of $Mg_3Al_2Si_3O_{12}$ pyrope is calculated at the Γ point by using the periodic ab initio CRYSTAL program that adopts an all-electron Gaussian-type basis set and the B3LYP Hamiltonian. The full set of frequencies (17 IR active, 25 RAMAN active, 55 silent modes) is calculated. The effect of the basis set and of the computational parameters on the calculated frequencies is discussed. It is shown that the mean absolute difference with respect to the experimental IR and RAMAN data is as small as 6 and 8 cm^{-1}, respectively. The IR and RAMAN modes are fully characterized by various tools such as isotopic substitution, direct inspection of the eigenvectors, and graphical representation. The present calculation permits to clarify some of the assignment and interpretation problems raised by experiment and previous simulations with force fields.

I. Introduction

Garnets are among the most important constituents of the Earth's upper mantle, and pyrope is probably the most important member of the family (see ref 1 and references therein). It is then not surprising that many experimental and theoretical efforts have been devoted to understanding its properties. Among these, a crucial role is played by vibration frequencies, which have been investigated by many authors: the single-crystal reflectance studies of Hofmeister et al.,[2] in 1996, that give a complete set of IR-active modes (17 modes); the RAMAN spectra by Hofmeister and Chopelas,[3] in 1991, by Gillet et al.,[4] in 1992, and by Kolesov and Geiger, in 1998[5] and 2000[6] (see ref 1 for experiments before 1990). As regards theoretical studies, the paper by Chaplin et al.[1] is worth mentioning, where the full set of frequencies at the Γ point is calculated. Other authors[7,8] computed the elastic constants and the full phonon spectrum, and explored the effect of pressure and temperature on the structural and dynamical properties. All of these simulations were based on semiempirical force-field or shell-model like schemes, the parameters of the models being obtained by best-fitting experimental data of simple oxides (MgO, Al_2O_3, and SiO_2).

The aim of the present paper is to show that the full vibrational spectrum[9] of pyrope can be calculated quantum-mechanically with CRYSTAL,[10] an ab initio, periodic, all-electron computer program that uses a Gaussian-type basis set for representing the crystalline orbitals. Our method, which is based on the calculation of the Hessian matrix by numerical differentiation of the analytical energy gradients with respect to the nuclear positions, proved to be effective in the calculation of the vibrational spectra of α-quartz. In fact, in previous papers,[9,11] the effect of the computational parameters controlling the accuracy of the calculated vibration frequencies of α-quartz, as well as basis set and Hamiltonian effects, was discussed at length, showing that the B3LYP[12] Hamiltonian provides frequencies that are very close to experiment (mean absolute difference of 6−7 cm^{-1}).

Garnets have a cubic structure ($Ia\bar{3}d$ space group) with formula $X_3Y_2Si_3O_{12}$; the SiO_4 tetrahedra share corners with the YO_6 octahedra (Y is a trivalent cation, Al in the present case); triangular-dodecahedral sites contain X cations, Mg in the present case. There are four formula units (80 atoms) in the primitive cell, originating 240 vibrational modes.

The structure of the paper is as follows. We first summarize the method employed in the calculation of vibrational spectra. The dependence of the calculated frequencies on the relevant computational parameters is then analyzed and compared to the case of α-quartz,[9] a semicovalent system with different structure and symmetry. The full calculated vibrational spectrum is presented in the Results section, along with an analysis of basis set effects and comparison with experiment.

II. Computational Methods

A development version of the CRYSTAL program[10] has been used for the present calculations. The B3LYP Hamiltonian[12] has been adopted, which contains a hybrid Hartree−Fock/density-functional exchange-correlation term and is widely and successfully used in molecular quantum chemistry[13] as well as in solid-state calculations, where it has been shown to provide geometries and vibration frequencies[11,14] in much better agreement with experiment than LDA or GGA.[11,15] In particular, B3LYP does not show the large overestimation of the H bond

* To whom correspondence should be addressed.
[†] Université Henri Poincaré.
[‡] Universidad Autónoma del Estado de Morelos.
[§] Università del Piemonte Orientale.
[||] Università di Torino.

10.1021/jp050316z CCC: $30.25
Published on Web 03/11/2005

TABLE 1: Effect of the Integration Grid on Energy, Geometry, and Vibrational Frequencies[a]

	(55 434)p	(75 974)p	(99 1454)p
N_p	636224	1781024	3487424
Δ_e	108	123	26
ΔE	−418	51	
α	11.5225	11.5222	11.5222
O_x	0.03251	0.03251	0.03251
O_y	0.05002	0.05005	0.05005
O_z	0.65354	0.65354	0.65354
Mg_1O	2.2048	2.2050	2.2049
Mg_2O	2.3576	2.3572	2.3572
AlO	1.8980	1.8980	1.8980
SiO	1.6442	1.6443	1.6443
$\lvert\bar{\Delta}\rvert$	0.6	0.7	
$\bar{\Delta}$	−0.1	−0.2	
Δ_{max}	1.8	−1.8	
Δ_{min}	−1.8	1.8	

[a] N_p is the number of points in the grid and Δ_e (in μ-electron) is the error in the integration of the charge density with respect to the number of electrons per cell (800 in the present case). ΔE is the energy difference (in μ-hartree) with respect to the reference (99 1454)p case (−11 430.377 108 5 Hartree), that can be considered as fully converged. a is the lattice parameter, O_i are the fractional coordinates of the oxygen atom. Mg_1O, Mg_2O, AlO, and SiO are distances in the cell (in Å). $|\Delta|$, $\bar{\Delta}$, Δ_{max}, and Δ_{min} are the average of the absolute difference, the average difference, the maximum, and minimum difference with respect to the reference case.

strength in OH groups and the related red shift of the OH stretching affecting most of the other functionals.[16,17]

The level of accuracy in evaluating the Coulomb and Hartree−Fock exchange series is controlled by five parameters,[10] for which standard values have been used (6 6 6 6 12). The DFT exchange-correlation contribution is evaluated by numerical integration over the cell volume.[9] Radial and angular points of the atomic grid are generated through Gauss-Legendre and Lebedev quadrature schemes. Grid pruning has been applied, as discussed in ref 9. Although the impact of the grid size on both the accuracy and the cost of the calculation has been discussed at length in previous papers,[9,14,15] pyrope is by far the largest system to which the present computational scheme has been applied. For this reason, the effect of the grid size on energy, geometry, and frequencies has been checked carefully, again, and the results are given in Table 1, where the notation $(n_r, n_\Omega)p$ indicates a pruned grid with n_r radial points and n_Ω points on the Lebedev surface in the most accurate integration region. Three grids have been considered, namely (55,434)*p*, (75,974)*p*, and (99,1454)*p*. The variability of the calculated vibrational frequencies ν_υ as depending on the integration grid is estimated through four global indices evaluated with respect to a reference set of frequencies ν_υ^{ref} as follows:

$$|\bar{\Delta}| = \sum_\upsilon |\nu_\upsilon - \nu_\upsilon^{ref}|$$

$$\bar{\Delta} = \sum_\upsilon \nu_\upsilon - \nu_\upsilon^{ref}$$

$$\Delta_{max} = \max(\nu_\upsilon - \nu_\upsilon^{ref})$$

$$\Delta_{min} = \min(\nu_\upsilon - \nu_\upsilon^{ref}) \quad \upsilon = 1, 2, ...$$

Table 1 shows that even our smallest grid provides quite accurate results for energy (0.4 mhartree higher than with the most accurate grid as a reference), equilibrium geometry (0.0003 Å difference in the lattice parameter), and frequencies (mean absolute error of less than 1 cm^{-1} with respect to the largest grids). This behavior is in line with previous results for α-quartz.[9]

TABLE 2: Calculated and Experimental Geometry of Pyrope[a]

	BSA	BSB	BSC	ref 31[b]
N	1440	1520	1820	
ΔE	0.20841	0.12536		
α	11.5222	11.54469	11.53346	11.439
O_x	0.03251	0.03214	0.032397	0.032907
O_y	0.05005	0.04971	0.049494	0.050688
O_z	0.65354	0.65344	0.653638	0.653311
Mg_1O	2.2050	2.2052	2.2028	2.1959
Mg_2O	2.3572	2.3648	2.3655	2.3335
AlO	1.8980	1.8987	1.8986	1.8850
SiO	1.6443	1.6496	1.6444	1.6337

[a] N is the number of basis functions (atomic orbitals) in the primitive cell. ΔE is the energy difference with respect the equilibrium total energy corresponding to BSC (−11 430.585 47 hartree). a is the lattice parameter (Å), and O_i are the oxygen fractional coordinates. Mg_1O, Mg_2O, AlO, and SiO are atom−atom distances (in Å). [b] $T = 30$ K.

The reciprocal space was sampled according to a regular sublattice with a shrinking factor IS equal to 2, corresponding to three independent **k** vectors in the irreducible Brillouin zone, with the use of such a small IS value being justified by the large size of the unit cell.

The gradient with respect to the atomic coordinates is evaluated analytically.[18−20] The equilibrium atomic positions are determined[21] by using a modified conjugate gradient algorithm as proposed by Schlegel.[22] Convergence in the geometry optimization process is tested on the root-mean-square (RMS) and the absolute value of the largest component of both the gradients and nuclear displacements. The threshold for the maximum and the RMS forces and the maximum and the RMS atomic displacements on all the atoms have been set to 0.000 045 and 0.000 030 au and 0.000 180 and 0.000 120 au, respectively. These values, which are 10 times smaller than usually adopted by us for geometry optimizations, provide a very accurate definition of the equilibrium geometry, that is crucial in the calculation of frequencies. The optimization is considered complete when the four conditions are satisfied simultaneously.

To discuss the basis set effect on the calculated geometry and frequencies, three all-electron basis sets of increasing size have been adopted. The simplest one,[23] to be denoted as BSA, contains 8-511G(d), 8-511G(d), 8-631G(d), and 8-411G(d) contractions for Mg, Al, Si, and O respectively; the exponent (in $bohr^{-2}$ units) of the most diffuse sp shells have been reoptimized for the present system and are 0.22 (Mg), 0.54 (Al), 0.32 (Si), and 0.25 (O). The exponents of the single Gaussian d shell are 0.5 (Mg), 0.5 (Al), 0.6 (Si), and 0.5 (O). An sp shell is added to Al (0.25) and Si (0.13) to form basis set B (BSB), whereas two sets of d functions are used for Si and O (the exponents are 2.56 and 0.54 for Si, and 2.0 and 0.41 for oxygen) in basis set C (BSC). The geometry and relative stability obtained with BSA, BSB, and BSC are given in Table 2, where it is shown that, despite considerable energy lowering from BSA to BSC, geometry modifications are extremely small, the difference with respect to experiment being 0.1 Å for the lattice parameter (less than 1%) and 0.01−0.02 Å for the quoted bond distances.

As regards the calculation of frequencies, we refer to a previous paper[9] for a more explicit formulation of the method. Here we simply remind that, within the harmonic approximation, frequencies at the Γ point have been obtained by diagonalizing

TABLE 3: Dependence of B3LYP Vibrational Frequencies of Pyrope at Γ on t_E (SCF Convergence Tolerance), *u* (Atomic Displacement for the Numerical Evaluation of the Hessian from the Analytical Energy Gradients), and *N* (Number of Total Energy Calculations along Each Nuclear Cartesian Coordinate for the Evaluation of the Hessian Matrix)[a]

		$\lvert\bar{\Delta}\rvert$	$\bar{\Delta}$	Δ_{max}	Δ_{min}
t_E	10	0.2	0.2	0.7	−0.6
u	0.003	0.4	−0.2	0.6	−0.9
N	3	0.1	0.0	0.3	−0.8

[a] $\lvert\bar{\Delta}\rvert$, $\bar{\Delta}$, Δ_{min}, and Δ_{max} are computed with reference to the frequencies evaluated with $t_E = 11$, $u = 0.001$ Å, and $N = 2$, respectively. For the three entries, only the indicated parameter has been modified with respect to the reference conditions.

the mass-weighted Hessian matrix *W*, whose (*i*, *j*) element is defined as $W_{ij} = H_{ij}/(M_iM_j)^{1/2}$, where M_i and M_j are the masses of the atoms associated with the *i* and *j* coordinates, respectively.

By the way, once the Hessian matrix *H* is calculated, frequency shifts due to isotopic substitutions can readily be calculated simply by changing the masses M_i in the above formula. In the present case, isotopic effects have been estimated for the substitution of ^{26}Mg for ^{24}Mg, ^{29}Al for ^{27}Al, ^{30}Si for ^{28}Si, and ^{18}O for ^{16}O. The natural abundance of ^{27}Al is 100%, so that ^{29}Al cannot be used in experiments. However, isotopic substitution is used here as an effective tool for identifying the ions contributing to the mode in a given frequency region.

Energy first derivatives with respect to the atomic positions, $v_j = \partial V/\partial u_j$, are calculated analytically for all u_j coordinates (u_j is the displacement coordinate with respect to equilibrium), whereas second derivatives at $\boldsymbol{u} = 0$ are calculated numerically using a single displacement ($N = 1$)

$$\left[\frac{v_j}{u_i}\right]_0 \approx \frac{v_j(0,\cdots,u_i,\cdots)}{u_i}$$

or averaging two displacements from the equilibrium coordinates ($N = 2$)

$$\left[\frac{v_j}{u_i}\right]_0 \approx \frac{v_j(0,\cdots,u_i,\cdots)\text{-}v_j(0,\cdots,\text{-}u_i,\cdots)}{2u_i}$$

The influence of either the number of points used in the evaluation of second derivatives ($N = 1$, 2) or the magnitude of the displacement u_i of each atomic coordinate ($u = 0.001$, 0.003 Å) on the calculated frequencies has been checked. Results are given in Table 3, which show that frequencies are nearly independent of both parameters ($\lvert\bar{\Delta}\rvert$ is as small as 0.2 and 0.4 cm^{-1}, respectively), so confirming the results of ref 9 also in this case.

Since the energy variations corresponding to the displacements considered here can be as small as 10^{-6}−10^{-8} hartree, the SCF cycle needs to be very well converged.

A corrective term should be added to the Hessian in order to obtain the TO-LO splitting for the F_{1u} modes.[9] Such a correction, however, has not been considered in the present case, as the implementation of the corresponding part of the program has not yet been completed.

Manipulation and visualization of structures have been dealt with the MOLDRAW program[24,25] and molecular drawings have been rendered by the PovRay program using input files prepared by MOLDRAW.

III. Results and Discussion

A. Basis Set Effects and Comparison with Experiment. The highly symmetric garnet structure contains 48 point-symmetry operators and belongs to the O_h point group. The decomposition of the reducible representation built on the basis of the Cartesian coordinates of the atoms in the unit cell leads to the following symmetry assignment of the 240 normal modes (this analysis is performed authomatically by the CRYSTAL code)

$$\Gamma_{total} = 3A_{1g} + 5A_{2g} + 8E_g + 14F_{1g} + 14F_{2g} + 5A_{1u} + 5A_{2u} + 10E_u + 18F_{1u} + 16F_{2u}$$

Totally, 17 modes are IR active F_{1u} (one F_{1u} corresponds to translations) and 25 are RAMAN active ($3A_{1g} + 8E_g + 14F_{2g}$). A total of 55 modes are inactive.

For completeness, the full set of 97 frequencies, calculated with BSB, is reported in Table 4, by increasing frequency and with symmetry classification, although the analysis is focused mainly on the IR and RAMAN active modes, where comparison with experimental data is possible.

We begin our analysis from the IR active modes by comparing the results obtained with the three basis sets (BSA, BSB and BSC) to each other and to the experimental data. The results by Hofmeister et al.[2] have been considered as a reference. Table 5 shows that there is a relatively large shift for many frequencies in going from BSA to BSB (whereas the corresponding changes in geometry are minor, as shown in Table 2), with a much better agreement with experiment in the case of the larger basis set. The absolute mean error, $\lvert\bar{\Delta}\rvert$, is 10.8 cm^{-1} with BSA, but reduces to 5.83 cm^{-1} with BSB, this value being similar to the value obtained for α-quartz[9] (7.9 cm^{-1}, that reduced to 5.8 cm^{-1} when also f orbitals were used) when using a sufficiently large basis set. The agreement is generally very good for all modes, with differences between calculated and experimental frequencies smaller than 7 cm^{-1} for all but 3 modes, for which the difference is +24 (674 vs 650), +13 (349 vs 336), and −13 (121 vs 134) cm^{-1}, respectively. At least two of these modes deserve, however, further discussion. In fact, the observed mode at 650 cm^{-1} is somehow uncertain (it is indicated as ∼650 in ref 2), and in their study dating 1991, Hofmeister and Chopelas[3] report about a TO mode at 664 cm^{-1}, which would agree with the present calculation much better and with the shell model simulation of Chaplin et al.,[1] as well, who predicted a mode at 681 cm^{-1}. If this peak is not included in the statistics, the mean absolute error for BSB decreases to +4.6

TABLE 4: Calculated Vibration Frequencies (cm^{-1}) of Pyrope and Symmetry of the Mode[a]

F_{2g}	106.5	F_{1g}	274.7	A_{1u}	377.8	B_u	521.0	F_{1u}	864.8
F_{2u}	118.1	F_{2u}	289.1	E_g	378.9	E_g	530.7	F_{2u}	867.7
F_{1u}	121.1	F_{1g}	290.4	F_{1u}	382.9	F_{1u}	532.8	F_{1g}	884.6
F_{1u}	139.8	E_u	300.3	F_{2g}	383.8	F_{2u}	536.3	F_{2g}	895.9
B_u	146.2	E_g	309.3	F_{1g}	384.5	E_u	562.4	F_{1u}	895.9
F_{1g}	155.1	B_g	310.2	B_u	395.7	A_{1g}	567.5	B_u	907.2
F_{1g}	168.5	B_u	311.8	F_{2u}	402.4	F_{1g}	579.6	E_u	911.0
F_{2g}	171.9	A_{1u}	313.7	F_{1u}	423.0	F_{1u}	582.9	F_{2u}	912.4
F_{1u}	189.3	F_{2g}	320.0	E_u	438.5	B_g	583.7	A_{1g}	923.8
F_{1g}	199.1	F_{1g}	325.7	B_g	448.3	F_{2g}	607.2	E_u	934.8
F_{2g}	204.2	F_{1u}	334.2	F_{2u}	452.7	E_g	635.8	E_g	936.3
F_{2u}	208.6	E_g	336.7	F_{1u}	459.0	F_{2u}	640.0	F_{2u}	953.6
E_g	209.2	F_{2u}	338.6	A_{1u}	467.7	F_{2g}	655.2	F_{1u}	969.7
E_u	210.5	F_{2u}	347.4	F_{1g}	476.9	F_{2u}	658.6	F_{1g}	970.9
F_{1u}	215.8	F_{1u}	348.6	F_{1u}	483.6	E_u	664.7	B_g	1028.5
F_{2u}	223.0	F_{1g}	349.6	F_{2g}	495.3	F_{1u}	674.1	A_{1u}	1047.4
B_g	238.1	E_u	350.7	E_u	501.5	A_{1u}	718.3	F_{2g}	1067.2
F_{1u}	259.9	F_{2g}	353.3	F_{1g}	506.0	F_{1g}	844.4		
F_{2g}	268.3	A_{1g}	356.5	F_{2u}	506.2	F_{2g}	860.6		
F_{2u}	270.2	E_u	375.8	F_{2g}	514.1	E_g	863.2		

[a] The modes are ordered by increasing frequency.

TABLE 5: Infrared-Active TO Modes (F_{1u}) of Pyrope as a Function of the Basis Set Size[a]

	calculated modes						
	BSA		BSB		BSC		observed
	ν	$\Delta\nu$	ν	$\Delta\nu$	ν	$\Delta\nu$	modes[2]
	987.6	+15.6	969.7	−2.3	964.3	−7.7	972
	912.6	+10.6	895.9	−6.1	890.3	−11.7	902
	882.0	+11.0	864.8	−6.2	859.1	−11.9	871
	691.4	+41.4	674.0	+24.0	672.8	+22.8	∼650
	594.1	+13.1	582.9	+1.9	580.7	−0.3	581
	538.2	+3.2	532.8	−2.2	532.4	−2.6	535
	504.5	+26.5	483.6	+5.6	481.2	+3.2	478
	470.7	+15.7	459.0	+4.0	457.3	+2.3	455
	427.7	+5.7	423.1	+1.1	422.9	+0.9	422
	390.4	+7.4	382.9	+0.9	382.7	−0.3	383
	352.5	+16.5	348.6	+12.6	349.2	+13.2	336
	337.5	+1.5	334.2	−1.8	334.7	−1.3	336
	261.4	+2.4	259.9	+0.9	258.9	−0.1	259
	219.8	−1.2	215.8	−5.2	216.6	−4.4	221
	192.5	−2.5	189.3	−5.7	190.6	−4.4	195
	141.9	+7.9	139.8	+5.8	140.4	+6.4	134
	133.1	−0.9	121.1	−12.9	120.3	−13.7	134
$\lvert\bar{\Delta}\rvert$	10.8 (8.9)		5.8 (+4.6)		6.3 (+5.3)		
$\bar{\Delta}$	10.2 (8.3)		0.8 (−0.7)		−0.6 (−2.0)		
Δ_{min}	−2.5(−2.5)		−12.9(−12.9)		−13.7(−13.7)		
Δ_{max}	+41.5(+26.5)		+24.1(+12.6)		22.8(+13.2)		

[a] Experimental data are also reported. Frequency differences ($\Delta\nu$) and statistical indices evaluated with respect to the experimental data (the values in parentheses correspond to excluding the mode at about 650 cm^{-1}, with uncertain assignment, from the statistics).

cm^{-1}. On the other hand, the peak at 134 cm^{-1} might be affected by temperature effects (the experimental spectrum was collected at room temperature) and approach the calculated frequency at low temperature (calculations refer to the 0 K limit). This is the case, for example, of the room-temperature RAMAN active mode at 136.5 cm^{-1}, which shifts to 127 cm^{-1} when the experiment is repeated at 4 K, see ref 6.

When more basis functions are added to Si and O atoms to give BSC, only minor adjustments are observed, the largest shift being smaller than 6 cm^{-1}; the mean absolute error increases slightly (from 5.8 to 6.3 cm^{-1}), but overall BSB appears to be already nearly complete.

In conclusion, an extremely good agreement with experiment is observed. As regards comparison with previous calculations, the results by Chaplin et al.,[1] although in overall qualitative agreement with the experiment, do not appear to approximate the vibrational spectrum equally well. In particular, they found a mode at 432 cm^{-1}, classified as T(Al), that is not present either in the experimental or in our calculated spectrum.

At variance with respect to IR measurements, many recent experimental RAMAN data are available: in 1991 Hofmeister and Chopelas[3] reported the full set of 25 RAMAN modes that appear in the last column of Table 7. A few complementary data reported by Chaplin et al.[1] as unpublished revisions by Hofmeister and Chopelas[3] (in parentheses in Table 7) are a clear indication of the difficulties encountered in identifying the low intensity modes, with the differences between the original and the revised frequencies being as large as 40 cm^{-1}. One year later Gillet et al.[4] reported a subset of 19 modes, whose frequencies were very close to the corresponding ones of ref 3 and that, for this reason, have not been reported in the table. More recently (1998), Kolesov and Geiger[5] published two new sets of data, the first set consisting of 17 modes only and referring to synthetic pyrope and the second set of 21 modes, but referring to natural pyrope (note that in Table 3 in ref 5, second column, one F_{2g} frequency is at 870.8 cm^{-1}, instead of 878.8; besides, the F_{2g} frequency at 222 cm^{-1} in Table 4, should be read as 212.5[26]). These two sets of frequencies coincide and are reported in column 8 of Table 7, along with the four additional frequencies of the second set, in parentheses. In the last column of Table 7 a set of 15 vibration frequencies refers to a spectrum collected by the same authors[6] at low temperature (4 K) two years later. Differences between room and low-temperature frequencies are all within the small range of 3 cm^{-1}, with the only noticeable exception of the lowest frequency mode that shifts from 136 to 127 cm^{-1}. Overall, all different sets of experimental data are consistent, with the exception of a few low intensity modes. For example, Hofmeister and Chopelas[3] report an E_g mode at 439 cm^{-1} which was not observed in other experiments and for which it is difficult to find any corresponding calculated E_g mode. Similar remarks apply to their F_{2g} mode at 285 cm^{-1}. Finally, they do not observe the low frequency F_{2g} mode at about 130 cm^{-1} that is reported both by Kolesov and Geiger[5] and in our calculated spectrum, at about 106 cm^{-1}. For these reasons, the statistical analysis of the calculated versus experimental data has been performed only for the 21 modes reported by Kolesov[5] (see last part of Table 7).

TABLE 6: Effect of the ^{26}Mg, ^{29}Al, ^{30}Si, and ^{18}O Isotopic Substitution on the Calculated IR-Active (TO) Modes (F_{1u} Symmetry)[a]

$Mg_3Al_2Si_3O_{12}$	^{26}Mg	^{29}Al	^{30}Si	^{18}O	
ν	$\Delta\nu$	$\Delta\nu$	$\Delta\nu$	$\Delta\nu$	assignment
969.7	−0.3	0.0	−12.4	−31.9	ν_3
895.9	−0.1	0.0	−11.2	−30.9	ν_3
864.8	−0.1	−0.1	−11.5	−28.9	ν_3
674.1	−1.1	−3.5	−4.4	−24.3	ν_4, T(Al)
582.9	−0.5	−7.4	−2.7	−15.6	ν_4, T(Al)
532.8	−0.1	−5.8	−3.8	−13.1	ν_4, T(Al)
483.6	−0.5	−1.3	−1.1	−21.9	ν_2
459.0	−0.3	−9.9	−0.4	−11.1	T(Al)
423.0	−0.2	−6.8	−2.4	−9.1	T(Al)
382.9	−0.2	−4.3	−1.0	−13.7	R(SiO_4), T(Al)
348.6	−0.1	−1.7	−1.6	−14.1	R(SiO_4)
334.2	−5.3	−0.8	−1.3	−8.4	T(Mg), T(SiO_4)
259.9	−3.4	−0.4	−1.8	−6.9	T(SiO_4), T(Mg)
215.8	−2.0	−0.9	−0.3	−7.9	T(SiO_4), T(Mg)
189.3	−5.7	−0.1	−0.5	−1.4	T(Mg)
139.8	−0.8	−0.5	−0.9	−4.8	T(SiO_4)
121.1	−3.7	−0.4	−0.1	−0.9	T(Mg)

[a] ν and $\Delta\nu$ in cm^{-1}.

Just like in the case of the IR data, the agreement with experiment improves in going from BSA to BSB, whereas BSC does not lead to any significant improvement. $|\bar{\Delta}|$ decreases from 13 to 7 cm^{-1}, and the largest difference is 30 cm^{-1} for the lowest frequency (it reduces to 21 cm^{-1} when the 4 K datum is considered). There is also another large discrepancy (308 vs 284 cm^{-1}) for a E_g mode, but this is a very low intensity mode (see Figure 2 in ref 5) for which Hofmeister and Chopelas proposed 309 cm^{-1} in their revision of the 1991 data[1], i.e., very close to our calculated frequency. When the comparison is performed with respect to the low temperature set (15 modes only) the agreement improves slightly ($|\bar{\Delta}|$ reduces to 5.8 cm^{-1}).

We conclude that also the calculated RAMAN vibration frequencies reproduce the experimental spectrum accurately, with $|\bar{\Delta}|$ for the full set of IR+RAMAN data between 6 and 7 cm^{-1}.

B. Mode Assignment. Site group analysis (SGA),[27] the correlation method,[28] and site group to factor group analysis[29] (FGA) of the garnet structure are usually applied in order to establish the relationship between mode symmetry and cation vibration. On the basis of such analyses, and taking into account the strong Si−O bond and the dominance of the interactions

TABLE 7: Observed and Calculated Raman-Active Modes of Pyrope (cm^{-1})[a]

	calculated modes						observed modes		
	BS A		BS B		BS C				
	ν	$\Delta\nu$	ν	$\Delta\nu$	ν	$\Delta\nu$	ref 5	ref 6	ref 3[b]
F_{2g}	1092.6	26.6	1067.2	1.2	1062.9	−3.1	1066.0	1066.1	1062
E_g	953.2	8.2	936.3	−8.7	929.8	−15.2	(945)		938
A_{1g}	945.4	17.4	923.8	−4.2	921.0	−7.0	928.0	926.6	925
F_{2g}	912.6	10.6	895.9	−6.1	889.7	−2.3	(902)		899
E_g	882.7		863.2		860.6				911(867)
F_{2g}	877.4	6.4	860.6	−10.2	854.5	−16.3	870.8	870.2	866
F_{2g}	679.3	29.3	655.2	4.6	653.5	2.9	650.6	648.2	648
E_g	648.8		635.8		634.9				626
F_{2g}	637.8	39.8	607.2	9.2	603.9	5.9	(598)		598
A_{1g}	585.4	22.4	567.5	4.7	564.6	1.8	562.8	561.4	562
E_g	551.5	26.5	530.7	5.7	528.7	3.7	525.0		524
F_{2g}	527.4	15.4	514.1	2.0	514.3	2.2	512.1	511.3	510
F_{2g}	508.0	16.0	495.3	2.9	493.8	1.4	492.4	491.6	490
F_{2g}	388.9	5.9	383.8	0.6	382.7	−0.5	383.2	383.6	379
E_g	386.7	11.7	378.9	3.9	379.2	4.2	(375)		365(379)
A_{1g}	368.0	4.0	356.5	−7.6	356.4	−7.7	364.1	363.4	362
F_{2g}	358.3	5.3	353.3	0.1	352.9	−0.3	353.2	352.1	350
E_g	343.3	−0.7	336.7	−7.8	337.4	−7.1	344.5	342.5	
F_{2g}	322.3	0.3	320.0	−2.0	319.7	−2.3	322.0	320.2	318(342)
E_g	312.6	28.6	309.3	25.3	308.5	24.5	284.0		342(309)
F_{2g}	272.4		268.3		268.6			273.0	272
F_{2g}	211.8	−10.2	204.2	−8.3	203.8	−8.7	212.5	209.4	230
E_g	212.6	1.6	209.2	−1.7	208.6	−2.3	210.9		203
F_{2g}	178.3		171.9		172.5				208
F_{2g}	121.9	−13.1	106.5	−30.0	106.0	−30.5	136.5	127.1	
$\lvert\bar{\Delta}\rvert$	13.9		7.0		7.6				
$\bar{\Delta}$	12.3		−1.3		−3.2				
Δ_{min}	−14.6		−30.0		−30.5				
Δ_{max}	39.8		25.3		24.5				

[a] $\Delta\nu$ is the difference with respect to the data in ref 5 that are also used for the calculation of the statistical indices at the bottom of the table (see text for definitions). The E_g mode at 439 cm^{-1} and the F_{2g} mode at 285 cm^{-1} reported by Hofmeister and Chopelas[3] have not been inserted in the table, because they do not correspond to any calculated frequency. [b] In parentheses unpublished revisions, as reported in ref 1.

between nearest neighbors, Hofmeister[3], Kolesov,[5] and Chaplin[1] classified IR and Raman active modes as symmetric and antisymmetric stretching (ν_1 and ν_3) or bending (ν_2 and ν_4) of the SiO_4 units, their rotations R(SiO_4) and translations T(SiO_4), as well as translations of the cations, T(Mg) and T(Al).

Such a partition is quite natural and effective as far as fully covalent or fully ionic subunits can be identified in the system like in $CaCO_3$,[14] for example, where the gap between inner modes and translation-rotation modes is larger than 300 cm^{-1}, although even in that case translation and rotation of the molecular fragment CO_3 interact with translation of the Ca cation strongly enough to give mixed modes (see the final section in ref 14). However, in the present case, a classification in terms of a "molecular fragment" (SiO_4) and "free" cations (Al, Mg) is a poor representation of the real system, because (a) the Al−O bond is almost as strong and covalent as the Si−O bond, and (b) due to the connectivity of the polyhedra around the three cations (Si, Al, and Mg) any distortion of one of them, for example, the bending of the tetrahedra, implies a corresponding distortion of the others (bending or stretching the octahedra), so that in most cases identifying cause and effect (the octahedra distorts as a consequence of the tetrahedra distortion, or viceversa) is a matter of taste. The arbitrariness of such a simple classification of the vibrational modes of pyrope in terms of subunits has been emphasized by several authors (see for example refs 3 and 1). In particular, when two or more nearly iso-energetic modes belong to the same symmetry species, as happens in this case particularly for low-frequency modes, mixing of the pure elementary modes is to be expected.

For this reason, we will proceed as follows: (a) we will give an overall description of the spectrum, that actually shows a large gap separating the Si−O stretching modes from the other modes; (b) we will refer to isotopic substitution for identifying the participation of the various atoms in the modes; (c) we will provide a graphical representation of the atom vibration in the 17 IR and 25 RAMAN modes, to enable the reader to classify the modes into simple categories (SiO_4 translation or rotation, and so on) as he wishes, although any such helpful classification ends to be a crude simplification in most cases.

The analysis of the full spectrum of the 97 modes (see Table 4) reveals the existence of a nearly continuum spectrum starting from 106 to 674 cm^{-1} (BSB data), with a large gap of about 170 cm^{-1} (from 674 cm^{-1}, F_{1u} symmetry, to 844, F_{1g} symmetry, see also Figures 1−4) separating these low-frequency modes from the upper 48 modes. A single A_u mode lies in the gap at 718 cm^{-1}.

Because in the unit cell there are 12 SiO_4 units, in the upper part of the spectrum 4 "molecular" modes per SiO_4 unit exist, that correspond to the asymmetric (3-fold degenerate in the isolated tetrahedra, with F_{2g} symmetry) and symmetric (A_{1g} symmetry) Si−O stretching, which were denoted as ν_3 and ν_1, respectively. These modes, being then quite far (in frequency) from all other modes, can be seen as "pure" stretching modes. Only three of the ν_3 3-fold degenerate modes are IR active; four ν_3 and two ν_1 modes are RAMAN active, as shown in Table 8; in the ν_1 symmetric modes the Si isotopic shift is null.

The effect of the isotopic substitution on all modes is shown in Figures 1−4; Figure 1 shows that Si participates essentially into modes above 844 cm^{-1}. Below 674 cm^{-1}, Figures 2 and 3 show that Mg and Al participate into modes at different frequencies, the former in the 100 to 300 cm^{-1} range, the latter in the 300−674 cm^{-1} range. Oxygen isotopic shift (Figure 4)

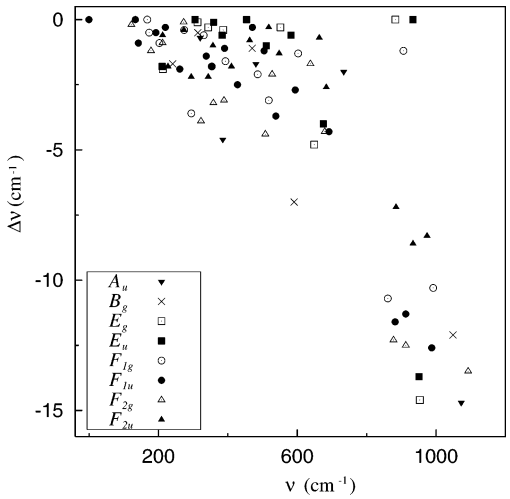

Figure 1. Isotopic shift $\Delta\nu$ on the vibrational frequencies ν of pyrope when ^{30}Si is substituted for ^{28}Si.

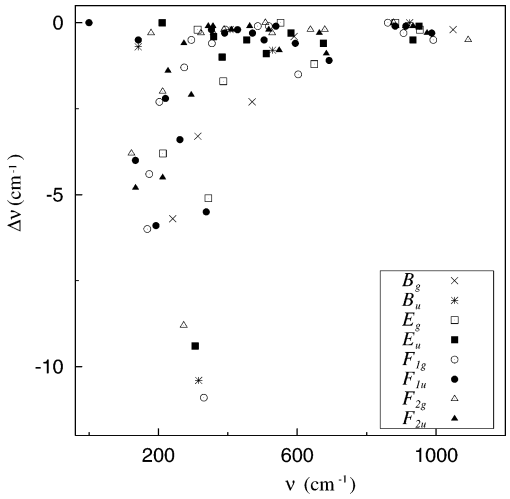

Figure 2. Isotopic shift $\Delta\nu$ on the vibrational frequencies ν of pyrope when ^{26}Mg is substituted for ^{24}Mg.

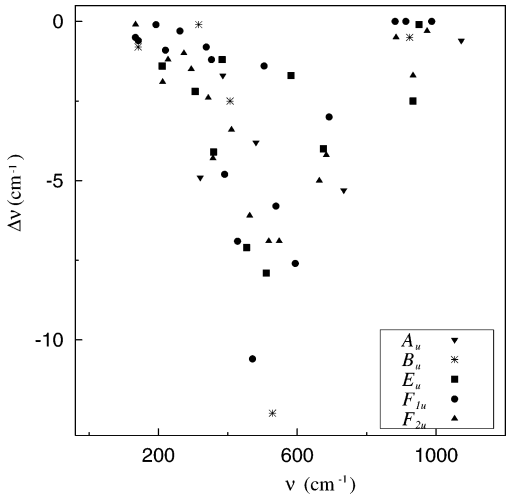

Figure 3. Isotopic shift $\Delta\nu$ on the vibrational frequencies ν of pyrope when ^{29}Al is substituted for ^{27}Al.

is important in the high-frequency modes, and decreases with the mode frequency, as expected. The frequency shift for the IR active modes is given in Table 6, where also a tentative classification of the modes according to the standard[27] nomenclature is reported.

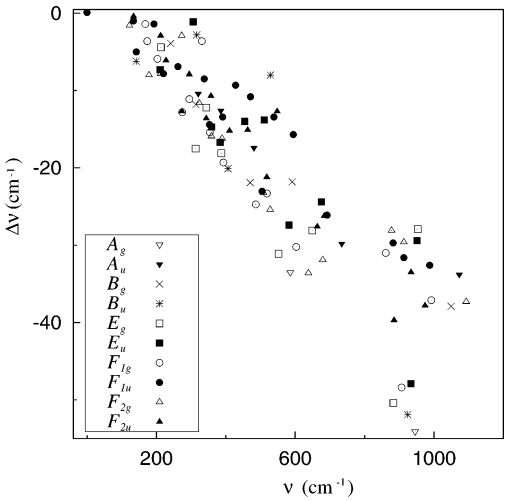

Figure 4. Isotopic shift $\Delta\nu$ on the vibrational frequencies ν of pyrope when ^{18}O is substituted for ^{16}O.

TABLE 8: Effect of the ^{26}Mg, ^{30}Si, and ^{18}O Isotopic Substitution on the Calculated Raman Modes (A_g, E_g, and F_{2g} Symmetry)[a]

	$Mg_3Al_2Si_3O_{12}$	^{26}Mg		^{30}Si	^{18}O	
RI	ν	$\Delta\nu$	$\Delta\nu$*	$\Delta\nu$	$\Delta\nu$	assignment
F_{2g}	1067.2	−0.5	−0.2	−13.2	−36.5	ν_3
E_g	936.3	−0.2		−14.3	−27.3	ν_3
A_{1g}	923.8	0.0	0.0	0.0	−52.9	ν_1
F_{2g}	895.9	−0.1		−12.3	−28.9	ν_3
E_g	863.2	0.0		0.0	−49.3	ν_1
F_{2g}	860.6	−0.1	0.0	−12.2	−27.4	ν_3
F_{2g}	655.2	−0.1	−0.6	−4.3	−30.3	ν_4
E_g	635.8	−1.2		−4.9	−27.4	ν_4
F_{2g}	607.2	−0.1		−1.7	−31.7	ν_4
A_{1g}	567.5	0.0	0.0	0.0	−32.5	ν_2
E_g	530.7	−0.1	0.0	−0.3	−30.0	ν_2
F_{2g}	514.1	−0.2	−0.3	−3.9	−22.1	ν_4
F_{2g}	495.3	−0.2	−0.4	−2.5	−25.2	ν_4
F_{2g}	383.8	−0.2	0.0	−3.3	−15.7	R(SiO_4)
E_g	378.9	−1.9		−0.4	−17.3	R(SiO_4), T(Mg)
A_{1g}	356.5	0.0	−0.1	0.0	−20.4	R(SiO_4)
F_{2g}	353.3	−0.4	0.0	−2.7	−16.2	R(SiO_4)
E_g	336.7	−4.8	−5.0	−0.2	−12.3	T(Mg), R(SiO_4)
F_{2g}	320.0	−0.3	−0.3	−3.9	−11.8	T(SiO_4)
E_g	309.3	−0.2	−10.0	−0.1	−17.3	T(SiO_4)
F_{2g}	268.3	−8.5		−0.1	−3.0	T(Mg)
F_{2g}	204.2	−1.8	−1.8	−0.9	−7.7	T(SiO_4), T(Mg)
E_g	209.2	−3.7	−2.8	−1.8	−4.4	T(SiO_4), T(Mg)
F_{2g}	171.9	−0.5		−1.2	−7.7	T(SiO_4)
F_{2g}	106.5	−3.4	−5.0	−0.1	−1.3	T(Mg)

[a] With Al in a centro-symmetric position, there is no Al isotopic shift for the Raman modes. ν and $\Delta\nu$ in cm^{-1}. $\Delta\nu$* is the isotopic shift observed by Kolesov et al[5].

The results for the Raman modes are given in Table 8, where also the data reported by Kolesov and Geiger[5] for ^{26}Mg are shown. It can be seen that calculated and experimental shifts are very similar, with one important exception concerning the assignment by Kolesov and Geiger of the largest shift to the E_g mode at 284 cm^{-1}, which is at 309 in our calculated spectrum, whereas the maximum shift in our data is predicted for the F_{2g} mode at 264 cm^{-1}. It has already been noted that the experimental intensity of the 284 cm^{-1} mode, for which we have registered also the largest discrepancy between calculations and experiment, is extremely low, making that particular assignment questionable. A tentative classification of the Raman modes is reported in the last column of Table 8.

Animations representing the 17 IR and 25 Raman active modes are available at the CRYSTAL web-site.[30] To make the animation as clear as possible, only a fraction of the unit cell has been represented, containing one AlO_6 octahedra and the six SiO_4 tetrahedra linked to it. However, as in many cases Mg ions are involved in the mode, additional animations are provided with a bigger fragment containing also six Mg ions.

IV. Conclusions

The present paper shows that quantum mechanical simulations can provide valuable information concerning the vibrational spectra of crystalline materials even with large a unit cell, where the agreement with available experimental data is very good. It is shown that simulation with the CRYSTAL code is complementary to the experimental information in many respects, including the assignment of low intensity modes, that is usually critical in the experimental work, the frequencies of silent modes and a clear characterization of the various vibrational modes.

References and Notes

(1) Chaplin, T.; Price, G.; Ross, N. *Am. Mineral.* **1998**, *83*, 841−847.
(2) Hofmeister, A.; Fagan, T.; Campbell, K.; Schaal, R. *Am. Mineral.* **1996**, *81*, 418−428.
(3) Hofmeister, A.; Chopelas, A. *Phys. Chem. Miner.* **1991**, *17*, 503−526.
(4) Gillet, P.; Fiquet, G.; Malézieux, J.; Geiger, C. *Eur. J. Mineral.* **1992**, *4*, 651−664.
(5) Kolesov, B.; Geiger, C. *Phys. Chem. Miner.* **1998**, *25*, 142−151.
(6) Kolesov, B.; Geiger, C. *Phys. Chem. Miner.* **2000**, *27*, 645−649.
(7) Mittal, R.; Chaplot, S.; Choudhury, N. *Phys. Rev. B* **2001**, *64*, 094302.
(8) Pavese, A. *Phys. Chem. Miner.* **1999**, *26*, 649−657.
(9) Pascale, F.; Zicovich-Wilson, C. M.; Gejo, F. L.; Civalleri, B.; Orlando, R.; Dovesi, R. *J. Comput. Chem.* **2004**, *25*, 888−897.
(10) Crystal03 user's manual. Saunders, V. R.; Dovesi, R.; Roetti, C.; Orlando, R.; Zicovich-Wilson, C. M.; Harrison, N. M.; Doll, K.; Civalleri, B.; Bush, I. J.; D'Arco, P.; Llunell, M.; Université di Torino, Torino, 2003.
(11) Zicovich-Wilson, C. M.; Pascale, F.; Roetti, C.; Saunders, V. R.; Orlando, R.; Dovesi, R. *J. Comput. Chem.* **2004**, *25*, 1873−1881.
(12) Becke, A. D. *J. Chem. Phys.* **1993**, *98*, 5648−5652.
(13) Koch, W.; Holthausen, M. C. *A Chemist's Guide to Density Functional Theory*; Wiley-VCH Verlag GmbH: Weinheim, Germany, 2000.
(14) Prencipe, M.; Pascale, F.; Zicovich-Wilson, C.; Saunders, V. R.; Orlando, R.; Dovesi, R. *Phys. Chem. Miner.* **2004**, *31*, 559−564.
(15) Tosoni, S.; Pascale, F.; Ugliengo, P.; Orlando, R.; Saunders, V. R.; Dovesi, R. *Mol. Phys.* **2004**, in press.
(16) Pascale, F.; Tosoni, S.; Zicovich-Wilson, C. M.; Ugliengo, P.; Orlando, R.; Dovesi, R. *Chem. Phys. Lett.* **2004**, *396*, 308−315.
(17) Ugliengo, P.; Pascale, F.; Mérawa, M.; Labéguerie, P.; Tosoni, S.; Dovesi, R. *J. Phys. Chem. B* **2004**, *108*, 13632−13637.
(18) Doll, K.; Saunders, V. R.; Harrison, N. M. *Int. J. Quantum. Chem.* **2001**, *82*, 1−13.
(19) Doll, K. *Comput. Phys. Comm.* **2001**, *137*, 74−88.
(20) Orlando, R. in preparation.
(21) Civalleri, B.; D'Arco, P.; Orlando, R.; Saunders, V. R.; Dovesi, R. *Chem. Phys. Lett.* **2001**, *348*, 131−138.
(22) Schlegel, H. B. *J. Comput. Chem.* **1982**, *3*, 214−218.
(23) Crystal basis set database. www.chimifm.unito.it/CRYSTAL/basis.html.
(24) Moldraw program. Ugliengo, P.; Viterbo, D.; Chiari, G. www.chimifm.unito.it/fisica/moldraw/moldraw.html.
(25) Ugliengo, P.; Viterbo, D.; Chiari, G. *Z. Kristallogr.* **1993**, *207*, 9−23.
(26) Geiger, C. Private communication.
(27) Moore, R. K.; White, W. B.; Long, T. V. *Am. Mineral.* **1971**, *56*, 54−71.
(28) Fateley, W. G.; Dollish, F. R.; McDevitt, N. T.; Bentley, F. F. *Infrared and Raman selection rules for molecular and lattice vibrations: the correlation method;* Wiley-Interscience: New York, 1972.
(29) Farmer, V. C.; Lazarev, A. N. *The Infrared Spectra of Minerals*; Mineralogical Society: London, 1974.
(30) Animation of pyrope normal vibration modes. www.crystal.unito.it/supplement/Frequencies/vibrational_modes.html.
(31) Pavese, A.; Artioli, G.; Prencipe, M. *Am. Mineral.* **1995**, *80*, 457−464.